Exploring the Relationship Between Land Surface Temperature and Air Temperature in Amsterdam, Netherlands: A Basis for the Continuous Spatial Estimation of Air Temperature

By

Pepijn Willem Herbermann

2747141

Bachelor's Thesis

Earth Sciences, Economics, and Sustainability

Faculty of Science

Vrije Universiteit Amsterdam

Under the guidance of Eric Koomen and Eduardo Simao Da Graca Dias

2025

Abstract

Urban heat poses growing challenges for cities, especially during summer. This study explores to what extent air temperature in Amsterdam can be explained using satellite-derived land surface temperature (LST), along with geospatial and meteorological variables. An additional objective was to assess whether this relationship could support spatially continuous estimates of urban air temperature. Using Landsat 8 and MODIS Aqua imagery from 2022–2024, we developed regression models separating LST into a daily mean and local deviation, capturing day-to-day and within-day spatial variation in temperature. Additional variables included NDVI, water fraction, albedo, population density, humidity, precipitation, and wind speed. Results show that mean LST is the strongest predictor, while local deviation remains important for identifying intra-urban heat patterns. The final models explained 75% of the variation in air temperature. The models including geospatial variables were applied in Google Earth Engine to generate spatially continuous air temperature estimation maps for Amsterdam. While no validation was performed, the outputs present the method's potential. This approach offers a scalable tool to support climate adaptation planning by identifying heat hotspots and providing information for neighbourhood targeted heat mitigation in urban areas.

Table of Contents

§1 Introduction

The damage caused by climate-related hazards, excluding the effect of climate change, is expected to triple by 2100 compared to 2008, as a result of economic development, population growth, and urbanisation (United Nations, 2010). The report highlights that between 1990 and 2008, heat-induced damages remained at 1 billion dollars annually. If no specific adaptive policies are implemented, the United Nations predict that the impact of heat-induced damages will increase thirty-fold to 31 billion dollars. Simultaneously, the sixth assessment report from the Intergovernmental Panel on Climate Change (2023) projected a significant increase in global temperatures by 2100. The damage, projected by the United Nations, will likely be intensified by the combined effects of urbanisation and climate change.

The Urban Heat Island (UHI) effect plays a crucial role in the spatial distribution and intensity of heat as a climate-related hazard and will be the main focus of this research. The Urban Heat Island effect refers to the temperature difference between urban areas and their surrounding natural or rural environments (Phelan et al., 2015). Clinton and Gong (2013) differentiate between meteorological UHI, which involves the warming of the air above urban areas, and surface UHI, which refers to increased land surface temperatures.

Summers in the Netherlands, which are no exception to global climate change, are becoming increasingly hot, with a rising number of extreme temperature events (KNMI, 2024). In urban areas, the UHI effect exacerbates this increase in temperature. For Amsterdam, the capital of the Netherlands, the results were severe and diverse, from dried-out plants to subsiding housing foundations and malfunctioning bridges. Most importantly, elevated temperatures pose significant health risks and, in extreme cases, can result in heat-related mortality. Multiple studies on other European cities found that the Urban Heat Island effect significantly increases death tolls during heat waves (Paravantis et al., 2017; Heaviside et al., 2016).

A large variety of data sources have been used to study the Urban Heat Island (UHI) effect, each with its strengths and limitations. Some approaches rely on mobile measurement devices (Koomen & Diogo, 2015), which are useful for spatial analysis but lack historical depth. Others use paired urban and rural air temperature sensors to capture the UHI. In recent years, the use of amateur meteorological data has grown, driven by the increasing number of personal weather stations (Meier et al., 2017). Surface Urban Heat Island (SUHI) intensity can also be calculated using thermal infrared sensors, either ground-based or mounted on satellites (Zhou et al., 2018).

Although satellite-derived LST data is both temporally and spatially abundant, it does not directly reflect human thermal experience. In contrast, air temperature is more directly associated with public health and thermal comfort (Naserikia et al., 2023). Therefore, understanding the extent to which LST approximates air temperature could be of great value.

Despite its relevance, there is little research on how well LST can serve as a proxy for spatially interpolated air temperature in Amsterdam. Case studies from various cities around the world (Scott et al., 2018; D. Li & Bou-Zeid, 2013; Schatz & Kucharik, 2015), as well as a global analysis by L. Li et al. (2020), all show that the relationship between LST and air temperature varies across space and time. These findings underline the need for regional case studies to provide data that can support locally adjusted policies.

This research addresses that gap by exploring the relationship between LST and air temperature in Amsterdam, using land surface temperature data derived from Landsat-8 and MODIS imagery in combination with meteorological data from amateur stations scattered throughout the city and its surrounding areas. A model is then developed to predict air temperature distribution based on satellite-derived LST.

Research Question:

To what extent can air temperature in Amsterdam be explained by land surface temperature (LST) and other relevant variables?

Subquestions:

1. What is the statistical relationship between air temperature and land surface temperature in Amsterdam?
2. To what extent do additional meteorological and spatial variables improve the explanation of air temperature variation across the city?

Objective:

An additional objective of this thesis is to apply the regression models to generate spatially continuous estimates of air temperature, using satellite and geospatial data.

Hypothesis:

The relationship is analysed using regression models, which are subsequently applied to generate spatially continuous air temperature estimates. It is hypothesised that LST, combined with other relevant variables, can substantially explain the variation in air temperature across Amsterdam.

§1.1 Literature review

This section provides a brief theoretical background for the thesis, highlighting key findings from the scientific literature. It discusses the urban heat island effect, the established determinants of urban temperature, and previous research on the relationship between LST and air temperature. These components form the conceptual basis for the statistical and predictive models developed in this research

The urban heat island effect refers to the tendency of urban areas to exhibit higher temperatures than surrounding rural or natural landscapes (Phelan et al., 2015). First described as early as 1833 by Luke Howard, the UHI effect is a long-recognised and highly researched phenomenon, and although it has been studied for nearly two centuries, our understanding of the effect has increased significantly in recent years, due to the increased focus on global warming and climate effects (Mohajerani et al., 2017).

The effect can largely be attributed to the following factors: decreased vegetation, lower surface albedo, urban geometry, and anthropogenic heat. Reduced vegetation limits evapotranspiration, reducing the cooling effect provided by plants. Surfaces with lower albedo, like asphalt and concrete, absorb and re-emit more solar radiation, adding to the energy input from the sun. The canyon-like urban geometry restricts airflow and traps heat. Lastly, human activity like transportation, central heating, and air conditioning releases waste heat, directly adding to the elevated temperatures in the city (Stone et al., 2010).

Researchers distinguish between two types of UHI: surface UHI, which refers to increased land surface temperatures, and meteorological UHI, which denotes elevated air temperatures (Clinton & Gong, 2013). Both forms are utilised in urban climate research; however, they are not interchangeable and can vary in magnitude and timing (Berg & Kucharik, 2021). Many studies on the UHI effect utilise satellite-derived surface temperatures due to the consistent global observations, whereas air temperature is only measured at meteorological stations, often limiting the spatial detail of the results (Naserikia et al., 2023). The limited spatial detail of meteorological UHI is inconvenient, given that air temperature is more directly linked to human health impacts and thermal comfort than surface temperature (Avashia et al., 2021). This distinction underlines the relevance of this study, which aims to explore the extent to which LST can explain air temperature in Amsterdam.

The air and surface temperatures in cities are the product of many interrelated factors. Li et al. (2020) broadly define these into two categories: urban design factors, such as vegetation cover, albedo, building density, and anthropogenic heat; and climate factors, including humidity, wind speed and direction, and cloud cover. Several of these variables, for example, NDVI and building density, affect both land surface and air temperature. This overlap introduces the potential for multicollinearity and mediation effects, which will be evaluated during the regression analysis. Incorporating these variables is essential for improving the explanatory power of the model and for better understanding the relationship between LST and air temperature.

First, the urban design factors. Vegetated land cover is known to reduce temperatures. For example, a study by Shiflett et al. (2016) found a substantial decrease in both air and land surface temperature in areas with high NDVI values. The Normalised Difference Vegetation Index (NDVI) is a common indicator of the amount of vegetation, which is calculated using the difference between near-infrared and red reflectance, divided by their sum. Albedo has been found to have a significant influence on both land surface and air temperature (Prado & Ferreira, 2004; Krayenhoff & Voogt, 2010). If a surface, such as a roof, has a high albedo, more light is reflected, and thus less energy is re-emitted as heat. Perini and Magliocco (2014) concluded that both the building density and the building height affect the air temperature. Whereas the building density positively impacted the air temperature, and the building height had a negative impact on air temperature, which they ascribed to the increased shading effect of tall buildings at street level. Lastly, anthropogenic heat is found to have an impact of up to 1.5°C in London, which has a fairly similar climate to Amsterdam, though it is a much larger city (Bohnenstengel et al., 2013). The effect was greatest in the winter season, as the anthropogenic heat influx was large relative to the incoming solar energy. Population density is commonly used as a first-order proxy for anthropogenic heat (e.g., Marcotullio et al., 2021), although it does not fully capture transport and industrial heat flux.

Second, the climate factors. Humidity plays an important role in modulating the strength of the UHI effect. A study by Zhao et al. (2014) found that in humid climates, the temperature difference between the city and the rural surroundings can be up to 3°C, whilst the difference can be negative (up to 1.5°C) in dry climates. The same study found convection between the surface and the atmospheric boundary layer to be crucial for the near-surface air temperature experienced by humans. The extent of this effect depends on both wind and surface roughness. Lastly, clouds absorb or reflect solar radiation, thereby determining the amount of radiation that reaches the surface (Alonso et al., 2007). Unfortunately, the land surface temperature can only be measured via thermal infrared sensors for cloud-free atmospheres, for clouds block the thermal infrared radiation from the surface. Consequently, data from cloudy days have been excluded from this study, and thus the effect of clouds is not included. In this study, a selection of these urban design and climate factors is incorporated into the regression models to assess their influence on air temperature and their interaction with LST.

A global analysis by L. Li et al. (2020) on the relationship between surface urban heat island intensity (SUHII), the difference in land surface temperature between urban and rural areas, and air temperature highlights the considerable variability of the urban climate. It must be noted that this study looks into the relationship between SUHII and air temperature, and not land surface temperature and air temperature; their results do clarify the need for localised research as the urban climate is a complex and spatially dependent system. A study by Stoll and Brazel (1992) on the relation between air and surface temperatures in Phoenix, Arizona, found strong correlations between the two temperatures where the land's surface temperature could explain more than 93% of the variation in air temperature. They also found that wind velocity significantly reduced the correlation between LST and air temperature in certain locations, lowering the explained variance from 90% to 60%. Other research on the relation between LST and air temperature points out that LST typically exhibits a larger temperature range than air temperature and has greater spatial variability by day (Arnfield, 2003). This is likely due to the phase difference between the air and the surface. Air, being gaseous, can more rapidly redistribute heat through

convection, whereas solid surfaces exhibit greater thermal inertia and slower heat transfer. The correlation between the temperatures is therefore improved at night, when microscale advection, the transfer of heat by the flow of a fluid or gas, is reduced (Voogt & Oke, 2003). In addition, the spatial resolution of satellite-derived LST maps influences their ability to capture small-scale urban temperature patterns (Weng, 2009). This is why this study combines MODIS imagery, which offers high temporal resolution and a coarser spatial resolution, which most likely better capture the smooth air temperature gradient, with Landsat imagery, which provides very fine spatial resolution, better suited for capturing small-scale temperature variation.

§2 Methodology

This thesis applies a two-stage methodological approach to assess the statistical relationship between air temperature and LST in Amsterdam, and to apply this relationship to generate spatially continuous estimates of air temperature across the city. It builds upon data gathered and matched in a separate thesis extension (Herbermann, 2025). In the first stage, three statistical regression models are developed to quantify the relationship between air temperature measured by amateur weather stations and various explanatory variables, like satellite-derived LST, land cover characteristics, and other weather conditions. Slightly different models are created for daytime (Landsat 8) and nighttime (MODIS Aqua) observations. In the second stage, the best applicable regression model is applied to estimate gridded air temperatures across Amsterdam. This enables the transformation of highly detailed satellite and additional geospatial data into continuous air temperature estimates. While these estimates are not validated, they provide a demonstration of how satellite-derived LST and other relevant variables can be used to map the spatial distribution of air temperature. The next section provides a summary of the data gathered in '*Urban Climate: Mapping Land Surface Temperature Combined with Air Temperature in Amsterdam, Netherlands'*, quality control methods, regression model specifications, and regression model application techniques in detail

§2.1 Data Sources

The data gathered is from the summer season (June 21 to September 21) for the years 2022 to 2024, a period selected due to the high frequency of extreme temperatures and the typical prevalence of urban heat islands in temperate latitude cities (Oke, 1982). Thus, during our selected timeframe, people experience decreased thermal comfort, and heat-related health issues are more prevalent. The region of interest (ROI) encompasses the city of Amsterdam, the Netherlands, and its surrounding semi-urban and natural areas. Besides the city and open water, note the presence of a port in the north-east of our ROI and the airport 'Schiphol' in the south-west.

In the thesis extension, Landsat 8 was selected as a data source for its high-resolution thermal infrared (TIR) bands. The bands have a spatial resolution of 100 meters, which is spatially interpolated by NASA to 30 meters to match its other bands. A drawback of Landsat 8 is its 16-day revisit cycle, at around 11:00 A.M., which strongly limits the amount of observations. MODIS Aqua was selected as a data source for its finished LST product, which provides daily worldwide coverage at 2:00 A.M. The gain in temporal resolution comes at the expense of spatial resolution, as MODIS has a spatial resolution of 1000 meters.

The data selection resulted in a total of 29 usable Landsat 8 observations and 277 usable MODIS Aqua observations. After selection, a stringent cloud mask was applied for Landsat 8 images to filter out individual cloudy pixels. This removed images that were completely clouded, and replaced clouds with no-data values for partially cloudy images. This process was unnecessary for MODIS, as the finished LST product was already filtered for clouds. In addition, a highly detailed water mask was applied to

both Landsat and MODIS data, as open water should be treated separately in the derivation of LST (Sobrino et al., 2008). In this study water is completely masked out of the LST maps, but its effect on air temperature is included as a separate geospatial variable.

The satellite data was complemented by hourly meteorological records from Wunderground's network of amateur weather stations. About 80 stations provided measurements of air temperature, humidity, precipitation, and wind speed. Satellite data input included daytime LST calculated from the TIR bands of Landsat 8 and the finished nighttime LST product from MODIS Aqua. The LST maps were matched to the corresponding meteorological observations obtained via the Wunderground API, using carefully constructed Python scripts for the alignment. The precise processing steps are described in the thesis extension and the results are depicted in **Figure 1** (Herbermann, 2025).

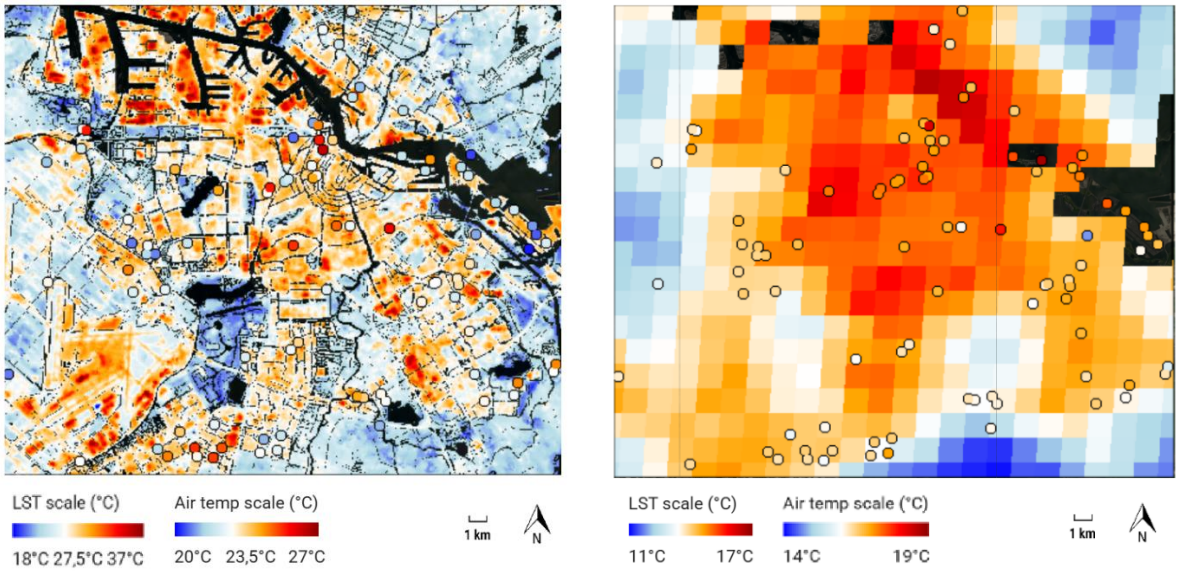

Figure 1. Median LST and air temperature measurements for Landsat 8 (left) and MODIS (right). Values are aggregated over the days for which satellite and meteorological data were available, so maps are mainly for display purposes. Furthermore, note the difference in temperature scales for the various data layers.

To assess the added explanatory power of environmental and spatial variables, additional datasets were incorporated based on their theoretical relevance to air temperature, as discussed in §1.1 (Theoretical Framework). The Normalized Difference Vegetation Index (NDVI) and surface albedo were derived directly from the Landsat 8 imagery. Built-up and surface water fractions were extracted from the ESA WorldCover 2021 land cover classification (Zanaga et al., 2021), while population density was sourced from the Dutch Bureau of Statistics dataset '*Kerncijfers wijken en buurten*.' (Centraal Bureau voor de Statistiek, 2025)

Using Google Earth Engine (GEE), circular buffers with radii ranging from 10 to 300 meters were applied around each weather station location. Within these buffers, mean values of LST, NDVI, albedo, built-up fraction, water fraction, and population density were calculated and matched to the corresponding meteorological records. These combined datasets form the basis for the regression analysis and subsequent spatial application of the model.

The last step before developing the regression model was to ensure the reliability of the amateur air temperature data used in this study. Amateur weather data is becoming increasingly popular in urban climate research due to its high spatial coverage (Meier et al., 2017). However, such amateur data can only be used when good quality control is applied, given the unprofessional nature, varying sensor placement, and inconsistent maintenance of the stations. Importantly, the reliability of amateur datasets can rely on the sheer number of measurement points, enabling the identification and filtering of specific odd measurements or entire odd measurement locations (Fenner et al., 2021). In this study, a five-step quality control process was implemented, outlined in the framework developed by Fenner et al.(2021). This process excluded data (1) from stations with duplicate or inaccurate locations, (2) that fell outside the 1^{st}-99^{th} percentile range for each day, (3) from stations with more than 20% of those invalid measurements over the whole summer, (4) from stations showing weak correlation ($r < 0.6$) with the median temperature of all readings, suggesting indoor placement, and (5) from station differing significantly from their neighbours in a 4.5 km range, based on a 'buddy check'. Even though a couple of stations were flagged due to the buddy check, we have chosen to exclude only station 'IAMSTE218' located in the western part of Amsterdam, due to its high deviation from the many neighbouring stations, being flagged for 16 out of 29 dates for Landsat 8. The other flagged stations were often located on the edge of the city near cooler areas with few neighbouring stations. Therefore, we deemed their deviation well-grounded and essential to keep to assess the influence of other variables like NDVI on air temperature.

Lastly, a threshold was applied to the LST to remove outliers. For Landsat 8, this threshold was set to 10°C, and for MODIS, to 2°C. The exact values were chosen based on the distribution of the measurements shown in **Figure 2** and **Figure 3**. The LST values under these thresholds are probably due to undetected clouds and should therefore be excluded.

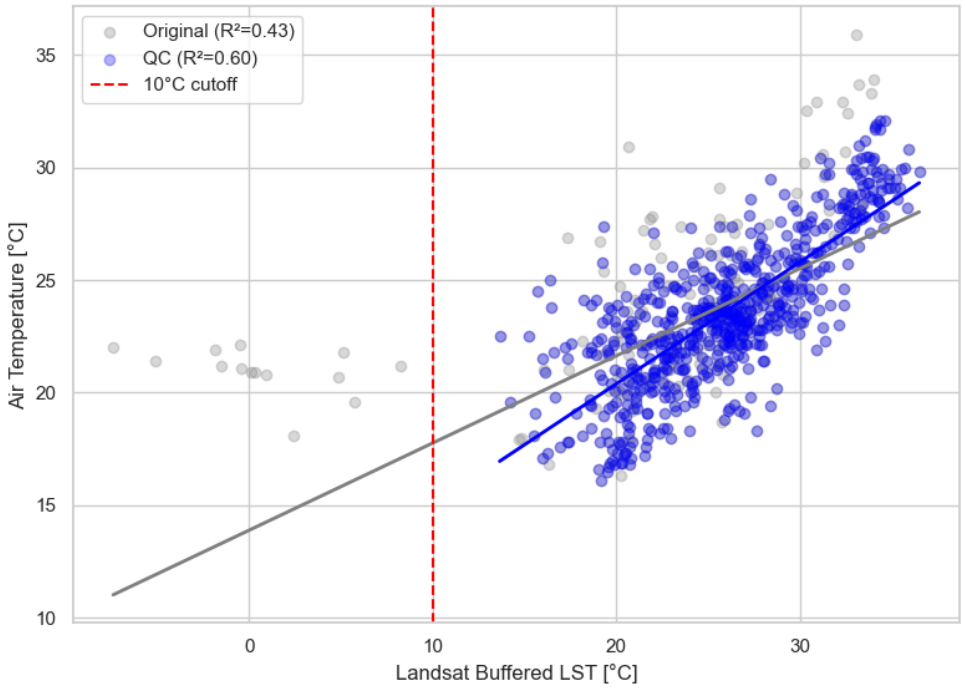

Figure 2: Landsat LST vs Air Temperature (100m buffer). Blue points show data after quality control (QC), while grey points represent the original data. The dashed red line marks the 10 °C LST cutoff applied to remove outliers. The R^2 value improves notably after QC, indicating better model fit.

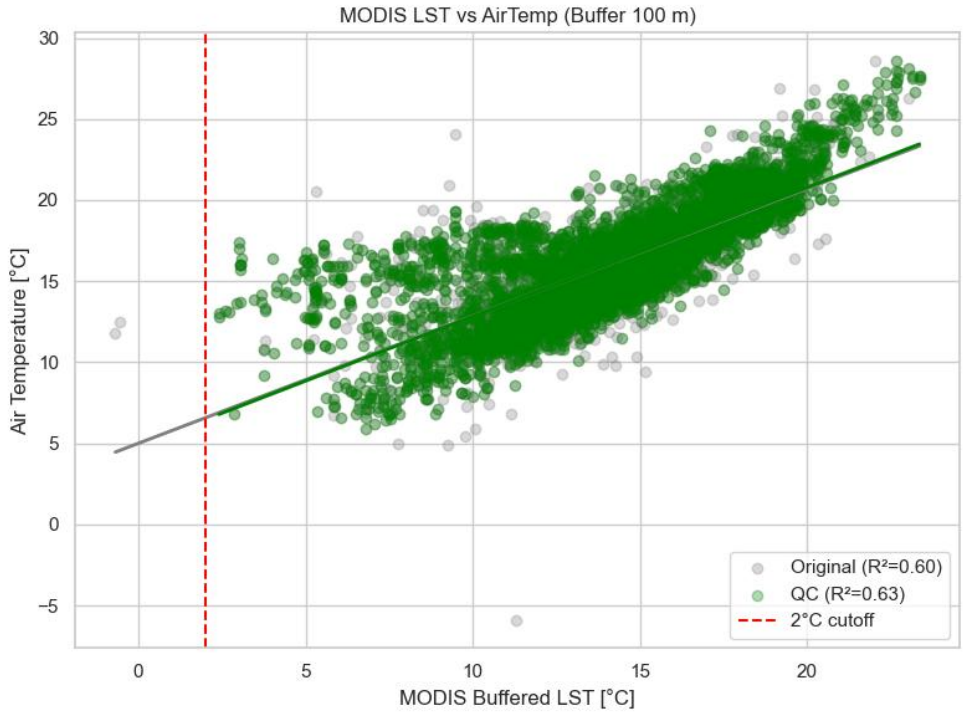

Figure 3: MODIS LST vs Air Temperature (100m buffer). Green points show data after quality control (QC), while grey points represent the original data. The red dashed line marks the 2 °C cutoff applied to filter out anomalously low LST values. The R^2 value improves notably after QC, indicating better model fit.

§2.2 Regression Model

LST can exhibit large spatial heterogeneity, varying by more than 10° Celsius over a space of just a few centimetres (Prata et al., 1995). On the other hand, air temperature is more spatially homogeneous due to atmospheric mixing and wind, which smooth out local variations. Consequently, LST and geospatial variables, such as NDVI and surface water, are likely to influence air temperature, not only directly overhead, but in an area surrounding it. This is supported by Shen et al. (2014), who found significant cooling effects of open water and urban green space extending up to 200 m and 500 m, respectively. Therefore, determining an appropriate buffer size around weather station locations is essential for linking air temperature measurements to LST and other spatial variables. An initial analysis was conducted to identify the optimal buffer size for this purpose..

Using a simple linear regression including all explanatory variables collected, buffer sizes were tested of 10, 25, 50, 100, 200, and 300 meters. The models were implemented in Python, and the performance was tested by R^2 value and the number of matched observations between air temperature and LST. Importantly, for daytime (Landsat 8) models, all spatial and meteorological variables were included. For nighttime (MODIS) models, we chose to exclude surface albedo, since we considered its effect on air temperature irrelevant during the absence of sunlight.

To better understand the relationship between land surface temperature (LST) and near-surface air temperature, LST was decomposed into two components:

- Mean LST, representing the citywide average LST at the time of the satellite overpass.
- Local LST deviation, representing the deviation of each station's LST from that daily mean.

This approach has two advantages. First, it allows the model to account for substantial inter-day variability in surface temperature, caused by weather conditions, cloud cover, or seasonality. Second, by explicitly separating the citywide thermal baseline, the model can better isolate and interpret the influence of local surface characteristics on air temperature.

Descriptive statistics (**Table 1**) confirm that both between-day and within-day LST variation are substantial. For example, Landsat mean LST (captured around 11:00 A.M.) ranges from 15.97 °C to 33.95 °C, with a standard deviation of 4.28 °C. The local LST deviation ranges from -8.66 °C to +4.5 °C. Similar variations are observed for the MODIS nighttime data. Although the between-day variation appears relatively smaller in comparison to Landsat daytime variation, whilst the within-day variation has a wider range with a smaller standard deviation compared to Landsat measurements. These large variations signify the need to model both broad temporal trends and fine-scale spatial differences to explain air temperature distribution effectively.

A similar approach was used by Berg & Kucharik (2021), who calculated LST and air temperature deviations by subtracting a citywide reference temperature from each observation. This allowed them to assess the local urban heat island intensity relative to a consistent thermal baseline, enabling clearer interpretation of spatial temperature patterns.

Variable	mean	sd	min	max	n
Air Temperature (°C)	16.24	3.23	5.90	28.60	6333
Mean LST (2:00 A.M.)(°C)	14.29	2.98	3.05	21.31	6394
Local LST Deviation (°C)	0.00	1.20	-10.66	6.08	6394

Variable	mean	sd	min	max	n
Air Temperature (°C)	23.58	3.25	16.10	32.10	640
Mean LST (11:00 A.M.)(°C)	25.89	4.28	15.97	33.95	640
Local LST Deviation (°C)	0.00	1.84	-8.66	4.50	640

Table 1: Descriptive statistics of air temperature, mean LST and local LST deviation for MODIS (left) and Landsat (right). The data is quality-controlled and gathered using a 100 m buffer.

Based on **Figure 4** and **Figure 5**, a buffer size of 100 meters was chosen for the final regression models. This choice is a compromise between maximising the number of matched observations and optimising model performance. Increasing the buffer size increases the likelihood that valid LST pixels fall within the buffer, which increases the number of matched observations between LST and air temperature. The amount of matches is particularly important for Landsat, where the data size is already limited due to the 16-day revisit cycle mentioned in §2.1. Limited data has a negative impact on the statistical robustness of the regression models. Furthermore, larger buffer sizes were also preferred because, as mentioned previously, air temperature reflects the influence of surrounding land surfaces, not just the exact point beneath the station

For Landsat, smaller buffer sizes slightly improved the model performance, whilst losing a large number of data matches. For MODIS, the model achieved its highest R^2 value at a 100 m buffer, and the number of matches was less relevant.

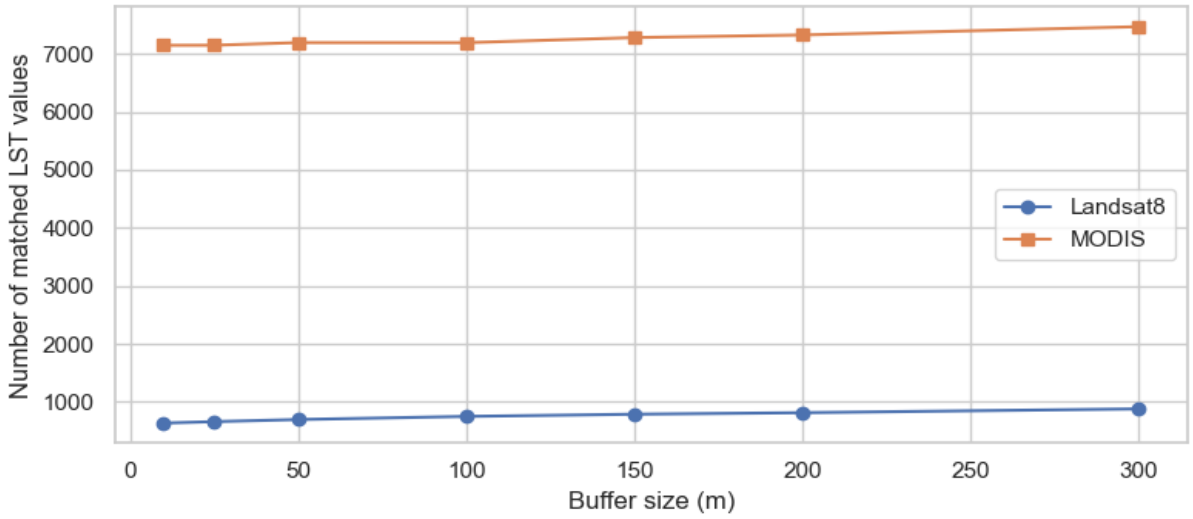

Figure 4: Number of air temperature measurements successfully matched to LST values at different buffer sizes. MODIS provides a much higher number of matches than Landsat due to its daily temporal resolution. Slight increases in match count with buffer size are visible for both sensors.

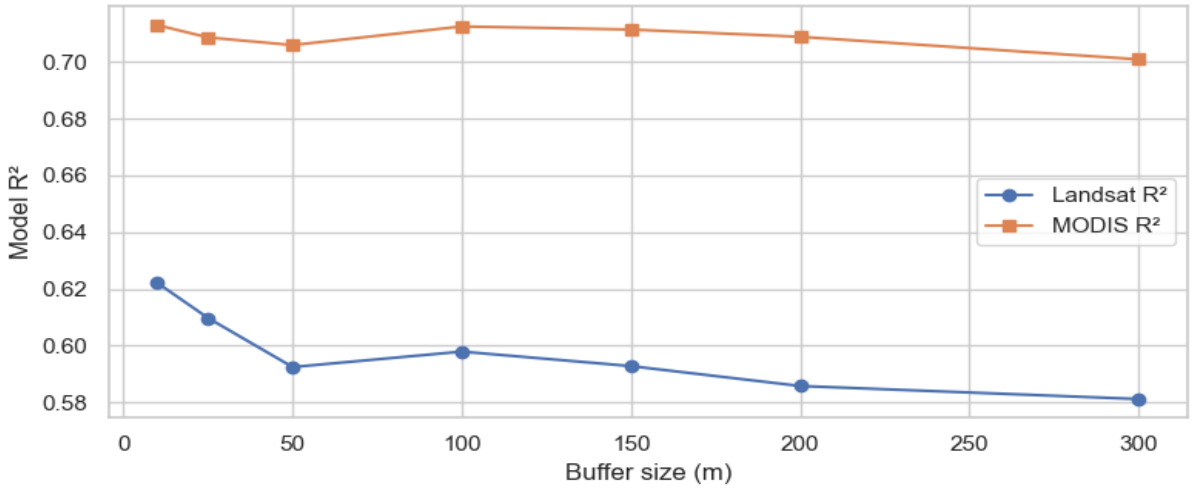

Figure 5: R^2 values plotted against buffer size. For Landsat, the model fit declines as buffer size increases, suggesting smaller spatial buffers better capture local thermal variation. MODIS shows relatively stable performance with a slight peak around 100 m.

Finally, to assess the statistical relationship between LST and air temperature, three regression models were constructed for both Landsat 8 and MODIS Aqua. Each model adds an extension to the previous model by incorporating explanatory variables, with the goal to evaluate the added value of spatial and meteorological variables on top of LST alone.

The models were estimated using ordinary least squares regression, with robust standard errors. As previously mentioned, daily mean LST was included in all models to control for daily variation in temperature and to serve as a temporal fixed effect. The value represents the average LST on a given date, and is subtracted from each buffered LST on the same date, to obtain the local LST deviation variable, representing the local variation from the daily mean. This distinction allows for a clear interpretation of spatial effects while adjusting for the broader temperature trend across the city.

The following models were formulated:

Basic Model:

$$Tair = \beta_0 + \beta_1 \cdot Local\ LST\ Deviation + \beta_2 \cdot Mean\ LST$$

This simple model serves as a baseline and tests whether differences in air temperature can be explained by deviations in the land surface temperature.

Static Model:

$$Tair = Basic\ Model + \beta_3 \cdot NDVI + \beta_4 \cdot Water + \beta_5 \cdot Albedo + \beta_6 \cdot Population\ Density$$

This model adds the static spatial variables, where NDVI is the average vegetation cover, water is the fraction of surface water in the buffer, albedo is the average diffuse surface reflectance in the buffer (**this parameter was excluded for MODIS)**, and population density is the average amount of people per square hectare that live in the buffer area. Note that built-up was excluded from the model, due to its high correlation with NDVI (-0.84 for MODIS and -0.81 for Landsat)

Weather Model:

$$Tair = Static\ Model + \beta_7 \cdot Humidity + \beta_8 \cdot Precipitation + \beta_9 \cdot Wind\ Speed$$

For Landsat**, linear effects of humidity**, precipitation, and wind speed were included. For MODIS, a **nonlinear effect of humidity** was added in the form of a squared humidity term, due to the observed U-shaped humidity and nightly air temperatures. Note that the weather data is based on hourly summaries. This enabled the inclusion of precipitation, whilst still applying a stringent cloud mask.

The models were fitted with the quality-controlled data and a buffer size of 100 meters, as previously justified. The performance of each model was summarised into regression tables, and coefficient plots with 95% confidence intervals were generated to assess the strength and uncertainty of the variables. Both can be found in the next section: §3 Results.

§2.3 Model application for air temperature estimation

To derive spatially continuous predictions of air temperature from satellite-derived land surface temperature, the regression models constructed in paragraph §2.2 were implemented in Google Earth Engine (GEE). This analysis environment enabled the combination of Landsat 8 and MODIS Aqua LST measurements, the geospatial variables, and the model coefficients into gridded air temperature estimates.

The prediction process was executed separately for Landsat and MODIS data to accommodate the use of different model parameters. For the prediction, the Static Model was used, as this model includes both spatial and thermal variables, but more importantly, does not contain meteorological variables. These are nearly impossible to gather at the spatial resolution of our entire region of interest.

For each satellite, a clear-sky image was selected to avoid gaps caused by cloud masks. From these images, the two thermal variables, mean LST and local LST deviation, were derived. Additionally, focal statistics with a 100 m radius were applied to the entire geospatial variable rasters. This method aligned our variables with the 100 m buffer size implemented during the matched data extraction process in §2.2, to capture the atmospheric mixing and the spatially extended impact of surface characteristics described in Shen et al. (2014). Albedo was excluded for MODIS-based predictions, as it is not expected to influence nighttime temperature in the absence of solar radiation.

The averaged variables and the thermal variables were stacked into a multiband image, and the regression coefficients obtained from the static regression model were applied pixel by pixel to estimate air temperature across the whole region of interest. The result was a fine-scaled (10 m) continuous air temperature estimate map, which was resampled to a 177 m resolution. This resampling is a necessary step to avoid overinterpreting the artificially fine resolution of certain input layers and match the resolution to the effective spatial footprint of the 100 m buffer used in both the training data and focal statistics.

§3 Results

This section presents the main findings from the statistical analysis and displays the continuous air temperature maps generated by applying the regression model to LST data. First, in §3.1, the regression results are discussed to assess the statistical relationship between air temperature, LST, and other relevant variables. Next, in §3.2, the spatially continuous air temperature maps resulting from the application of the static regression model are presented. The maps demonstrate how satellite-derived LST combined with supplementary geospatial variables can be used to estimate air temperature across the region of Amsterdam.

§3.1 Regression Output

The regression results (**Table 2**) indicate a strong statistical relationship between LST and air temperature in Amsterdam. For both day (11:00 A.M. Landsat) and night (2:00 A.M. MODIS), the variable local LST deviation shows a consistent positive relation across all models. For MODIS, the effect is highly significant ($p < 0.001$), while for Landsat, the effect is only marginally significant ($p < 0.1$) for the static and weather models but significant in the basic model. In addition, mean LST, capturing the thermal baseline, also shows a positive and statistically highly significant relationship ($p < 0.001$) with air temperature over all models for both MODIS and LST. The coefficients of mean LST are considerably larger than those of local LST deviation. The coefficients show that a 1°C increase in mean LST results in a 0.6-0.8°C increase in air temperature, whereas a 1°C increase in local LST deviation only contributes to a 0.08-0.25°C increase in air temperature. This is likely due to the difference in LST range during the day and night.

From Table 2, it is clear that every regression model progressively adds explanatory power. The basic model, containing only mean LST and local LST deviation, already explains 67% (Landsat) and 68% (MODIS) of the variation in air temperature. Introducing the geospatial variables: NDVI, water fraction, albedo (Landsat only), and population density (per hectare), improves the R^2 slightly. At the same time, the coefficient for local LST deviation drops notably. This suggests that part of the spatial variation initially captured by local LST deviation can actually be explained by these static land surface characteristics. Finally, the weather model, which adds humidity (squared for MODIS), precipitation, and wind speed, improves the R^2 to 0.749 for Landsat and 0.732 for MODIS. Notably, the coefficient for mean LST decreases in this model. This probably indicates that part of the daily temperature variation captured by mean LST is better explained by these added weather conditions.

	Basic	Static	Weather
Local LST deviation (°C)	0.112**	0.092+	0.078+
	(0.042)	(0.053)	(0.045)
Mean LST (°C)	0.620***	0.619***	0.449***
	(0.019)	(0.019)	(0.032)
NDVI		1.023	0.834
		(1.072)	(0.920)
Water frac		-1.867**	-0.193
		(0.718)	(0.656)
Albedo		-9.796	-9.333
		(6.205)	(5.784)
Pop density (people/ha)		-0.000	-0.001
		(0.001)	(0.001)
Humidity (%)			-0.070***
			(0.013)
Precip rate (mm/h)			0.259***
			(0.077)
Wind speed (m/s)			-0.214***
			(0.032)
Num. Obs.	640	640	608
R^2	0.669	0.674	0.749

+ p < 0.1, * p < 0.05, ** p < 0.01, *** p < 0.001

	Basic	Static	Weather
Local LST deviation (°C)	0.255***	0.159***	0.122***
	(0.024)	(0.025)	(0.025)
Mean LST (°C)	0.884***	0.885***	0.837***
	(0.012)	(0.012)	(0.012)
NDVI		-1.105***	-1.503***
		(0.274)	(0.259)
Water frac		1.614***	1.171***
		(0.193)	(0.184)
Pop density (people/ha)		0.005***	0.003***
		(0.000)	(0.000)
Humidity²			-0.000***
			(0.000)
Precip rate (mm/h)			0.023***
			(0.006)
Wind speed (m/s)			0.157***
			(0.011)
Num. Obs.	6333	6333	5901
R^2	0.676	0.693	0.732

+ p < 0.1, * p < 0.05, ** p < 0.01, *** p < 0.001

Table 2: Regression analysis Results. Three models were fitted: Basic, Static, and Weather with Landsat 8 (left) and MODIS Aqua (right) land surface temperature data to assess relationship between air temperature and land surface temperature combined with other relevant variables.

Besides the thermal predictors, several geospatial and meteorological

variables contribute to explaining variation in air temperature. **NDVI,** representing vegetation cover, has large negative and statistically significant coefficients in all MODIS models. This aligns with the literature, which generally finds that vegetation mitigates heat via evapotranspiration and shading (during the day). For the Landsat model, however, a positive relation was found. However, the relation is not statistically significant.

The water fraction shows a strong, significant negative relation with air temperature in the Landsat static model but is non-significant in the weather model. For MODIS, the opposite effect is found: water fraction has a significant positive coefficient across all models. This duality is also expected, wherein water has a cooling effect during the day and a warming effect during the night due to the heat retention by water bodies, which are prominently present in Amsterdam.

Albedo is only included in the Landsat models, where it is found to have a very strong negative but statistically insignificant relation with air temperature. The negativity of the relation is expected, as higher albedo reflect more sunlight and reduces available energy. It remains unclear what led to the large confidence interval of the coefficient.

Population density (people per hectare) shows a very small and statistically significant positive effect on air temperature in all MODIS models. In the Landsat model, there is little to no effect with a large confidence interval, suggesting that anthropogenic heat sources contribute more clearly to nighttime temperatures

The meteorological variables were all found to have highly significant statistical relationship with air temperature. **Humidity** (squared for MODIS) is found to have a tiny negative impact for both Landsat and MODIS. **Precipitation rate** is found to have a sizeable positive effect on air temperature, which is unexpected as rain is generally considered to cool down air temperature. And **wind speed** is shown to have a cooling effect during the day, whilst it has a warming effect during the night, which could possibly be explained by on-shore winds with sea surface temperatures as high as 20°C (KNMI, 2025).

Due to the number of explanatory variables and models, coefficient plots (**Figure 6**) have been created from the regression table to aid in interpretation.

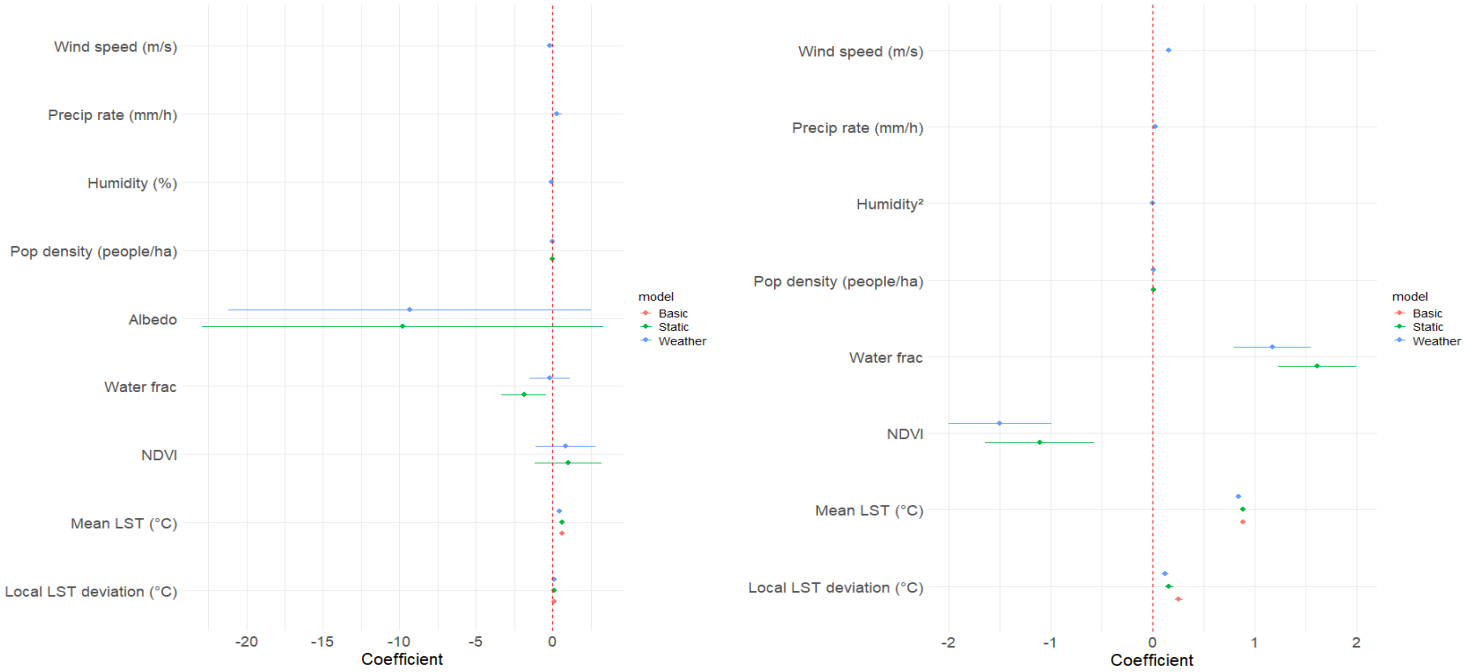

Figure 6: Coefficient plots for the Landsat (left) and MODIS (right) regression models. The plots visualize the coefficients and their 95% confidence intervals (horizontal bars) for the variables across all the models. The plots highlight differences in coefficient size, direction and significance. If the confidence interval bar does not cross red line, it is considered statistically significant.

§3.2 Spatial Application of the Regression Model

For comparison, the air temperature estimations (**Figure 7 & 8**) are displayed in combination with the specific satellite images used for their estimation. The maps provide insight into how the model translates LST and geospatial variables into the distribution of air temperature. Whilst the estimations are not validated against withheld observations or the real air temperature measurements for the day, they demonstrate the potential of satellite data, complemented with geospatial variables, to estimate continuous urban temperatures at fine resolution.

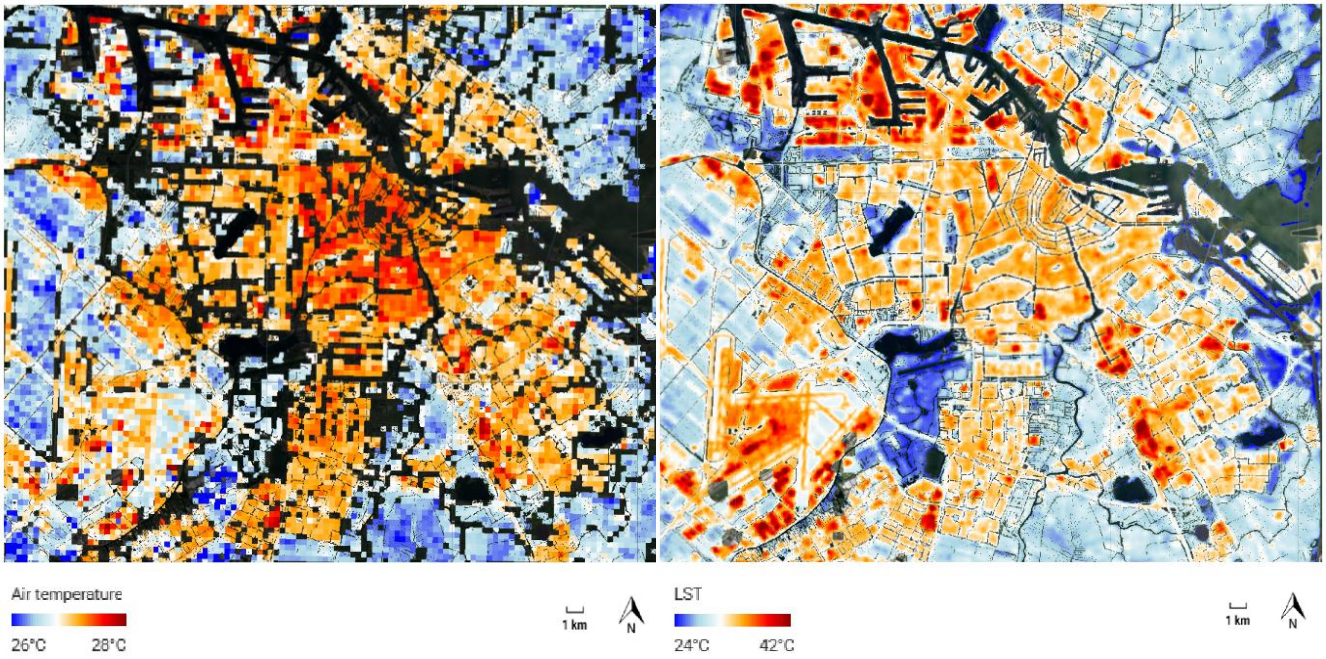

Figure 7: Landsat LST (right) and air temperature estimation (left). The temperature scales ranges differ significantly. The maximum difference in air temperature is 2°C, whilst the difference in LST is 18°C. Note that the city centre has the highest air temperature, whilst the (air)port have the highest LST. The Landsat image was taken at 2023/07/08 11:00 A.M.

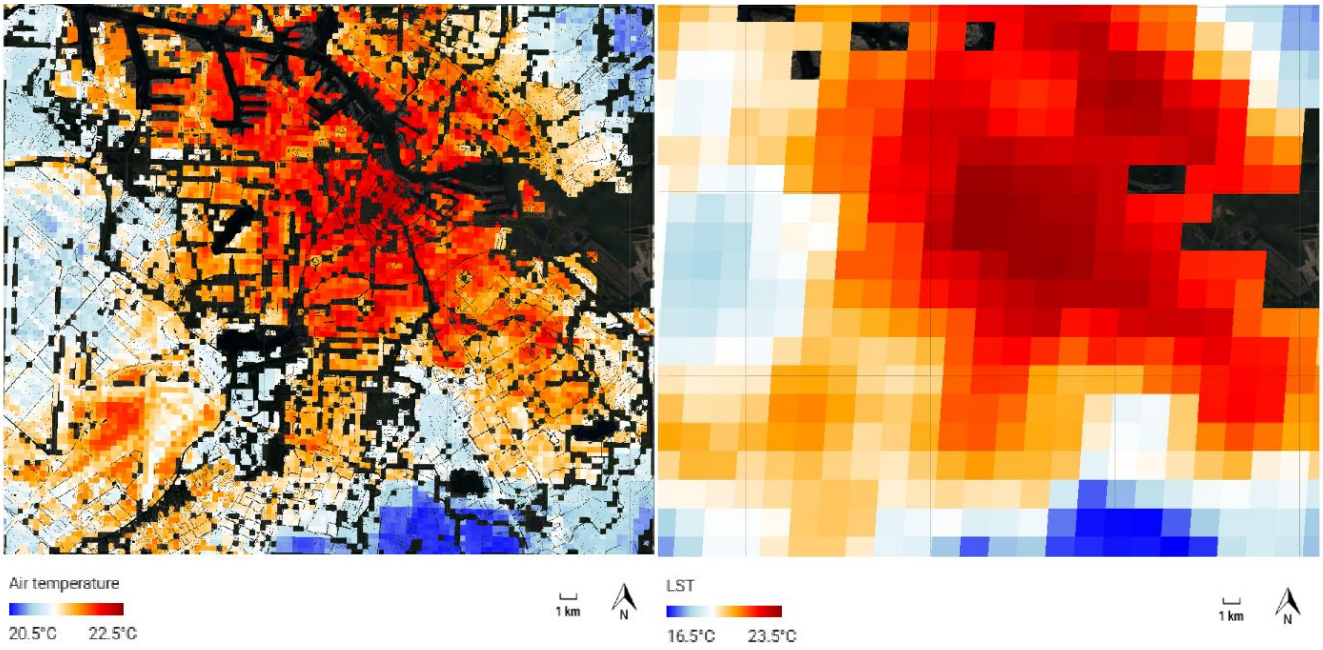

Figure 8: MODIS LST (right) and air temperature estimation (left). The temperature scales ranges differ significantly. The maximum difference in air temperature is 2°C, whilst the difference in LST is 7°C. Note that the distribution of temperatures is similar. The prevalence of water in the city centre increases the air temperature. The MODIS image was taken at 2022/07/20 2:00 A.M.

§4 Discussion

The purpose of this study was to assess to what extent air temperature in Amsterdam can be explained by land surface temperature (LST) and a set of relevant geospatial and meteorological variables. Our results confirm that LST is a strong predictor of air temperature, with statistically significant relationships found for both daytime (Landsat) and nighttime (MODIS) models, aligning with previous findings (Stoll & Brazel, 1992; White-Newsome et al., 2013). Through separating LST into a region-wide mean and local deviation, our findings indicate that broad-scale thermal variation, captured by mean LST, drives most of the daily differences in air temperature. However, local LST deviation also has a sizeable and significant relationship with air temperature, and plays a major role in explaining the spatial distribution of air temperature within the city.

The inclusion of additional variables improved the model. They were found to have diverse effects on air temperature in Amsterdam in both size and direction (**Table 2/Figure 6)**. Both NDVI and albedo were found to have cooling effects, aligning with previous studies (Shiflett et al., 2016; Krayenhoff & Voogt, 2010). Notably, NDVI showed a stronger relationship with air temperature during the night, which was also noted in the study of Shiflett et al. (2016). Water fraction was found to have a dual effect, cooling during the day and warming during the night, likely due to the thermal inertia of the water. Population density was found to have a very small positive impact on air temperature during the night, which aligns with previous studies (Khanh et al., 2025).

The meteorological effects were all highly significant and added a large amount of explanatory value to the models, with the full model explaining up to 75% of air temperature at 11:00 A.M (Landsat). The directions of the effects were mostly expected, except for precipitation, which was found to have a positive association with air temperature, potentially due to measurement timing and cloud-masking. These findings underline the value of combining LST with geospatial and meteorological variables to better understand and estimate air temperature in Amsterdam.

The global analysis by L. Li et al. (2020) highlights the considerable variability of the urban climate. Therefore, the results of this Amsterdam-specific study offer practical insights for urban planning and climate adaptation in the municipality. The spatially continuous air temperature maps derived from LST and geospatial variables can support policy decisions by identifying areas vulnerable to high air temperatures at fine resolution. This fits well with existing plans like the *Omgevingsvisie Amsterdam 2050* (Gemeente Amsterdam, 2021) and the city's Climate Adaptation Strategy (Gemeente Amsterdam, 2020), which both emphasize the need for more greenery, cooling measures, and a better living environment.

By linking heat patterns to land use characteristics, the approach enables more informed decisions based on how well common interventions, like increasing vegetation cover or creating more open water helps mitigate heat stress specifically for Amsterdam. The method also highlights how data from satellites can be applied locally to address heat inequality and climate resilience, supporting evidence-based planning for Amsterdam’s diverse neighbourhoods.

This study was conducted on data from the summer seasons in Amsterdam. As a result, the findings cannot be extended to any other season or location without further analysis. In addition, the 16-day revisit cycle strongly limits the amount of observations compared to MODIS (640 vs 6444 observations), which likely contributes to the lower statistical significance of the Landsat model coefficients. The overpass time of both satellites is also a constraint. Landsat captures Amsterdam around 11:00 A.M. and MODIS at approximately 2:00 A.M., missing both the minimum and maximum air temperature peaks, typically occurring in the early morning and late mid-day. These snapshots may not be representative of the entire night and day situation.

The weather data come from a network of amateur weather stations. While quality control was applied, incorrect sensor placement and maintenance may still weaken the regression output. The data could only be retrieved at an hourly resolution, which might be insufficient to capture short events like summer rainfall. Precipitation can evaporate quickly, especially in the summer, which could weaken the observed effect. Moreover, the spatial estimations were not validated against withheld measurements, thus predictive strength remains uncertain.

Despite these limitations, the study provides a robust framework for estimating urban air temperature using remote sensing and geospatial data, which can be improved and expanded in future research.

§5 Conclusions and Recommendations

This study demonstrates that LST, combined with geospatial and meteorological variables, can effectively explain variation in air temperature in Amsterdam. The findings confirm that LST is a strong predictor of air temperature, as both the thermal baseline (mean LST) and local deviation (local LST deviation) contribute significantly. Mean LST consistently showed strong and highly significant coefficients, implying that broader weather variation is the dominant factor in determining daily air temperature levels. Simultaneously, local LST deviation was found to be an important factor in determining spatial differences in air temperature.

Including the additional variables, NDVI, water fraction, albedo, population density, humidity, precipitation rate, and wind speed, further improved the models, with explained variance reaching 75% for Landsat and 73% for MODIS models. However, these findings are specific to summer conditions and based on data from Amsterdam. The regression model was successfully applied to generate spatially continuous estimates of air temperature. Since no validation of the estimates was performed, the results should only be interpreted as a showcase of this method's potential.

Future research could work on implementing the regression models on datasets gathered for different cities in the Netherlands, like Rotterdam or Utrecht, to compare the explainability of air temperature by LST and other variables city-wise. This could help tailor heat mitigation measures to each city's individual needs. Moreover, a follow-up study should validate the air temperature estimates on new data from e.g., the summer of 2025, to determine model accuracy. Adding the extra year of data would also be especially valuable for the Landsat models, since the 16-day revisit cycle greatly reduced the number of observations for this study, which resulted in some insignificant relationships. Finally, due to the complex interaction between variables, the use of other machine learning models, such as random forests or neural networks, could improve continuous air temperature estimation.

Based on this study, several recommendations can be made for local policy. The high-resolution continuous air temperature maps can be used to identify neighbourhoods with high air temperatures. The air temperature map can also be overlaid with socio-economic data to highlight economically fragile neighbourhoods that suffer from heat-stress, and might be unable to afford air-conditioning. Policies from the *Omgevingsvisie Amsterdam 2050* and the *Climate Adaptation Strategy* could incorporate this spatial data to target mitigation to the hottest areas first. The findings from this study imply that increasing NDVI, albedo (for daytime air temperatures) and the amount of open water, helps in lowering the air temperature. Finally, the maps could be used to support extreme heat plans and better prepare emergency services for extreme heat events.

References

Alonso, Fidalgo, & Labajo, J. (2007). The urban heat island in Salamanca (Spain) and its relationship to meteorological parameters. *Climate Research*, *34*, 39–46. https://doi.org/10.3354/cr034039

Arnfield, A. J. (2003). Two decades of urban climate research: a review of turbulence, exchanges of energy and water, and the urban heat island. *International Journal Of Climatology*, *23*(1), 1–26. https://doi.org/10.1002/joc.859

Avashia, V., Garg, A., & Dholakia, H. (2021). Understanding temperature related health risk in context of urban land use changes. *Landscape And Urban Planning*, *212*, 104107. https://doi.org/10.1016/j.landurbplan.2021.104107

Berg, E., & Kucharik, C. (2021). The Dynamic Relationship between Air and Land Surface Temperature within the Madison, Wisconsin Urban Heat Island. *Remote Sensing*, *14*(1), 165. https://doi.org/10.3390/rs14010165

Bohnenstengel, S. I., Hamilton, I., Davies, M., & Belcher, S. E. (2013). Impact of anthropogenic heat emissions on London's temperatures. *Quarterly Journal Of The Royal Meteorological Society*, *140*(679), 687–698. https://doi.org/10.1002/qj.2144

Centraal Bureau voor de Statistiek. (2025, 27 maart). *Kerncijfers wijken en buurten 2024*. Centraal Bureau Voor de Statistiek. https://www.cbs.nl/nl-nl/maatwerk/2025/13/kerncijfers-wijken-en-buurten-2024

Clinton, N., & Gong, P. (2013). MODIS detected surface urban heat islands and sinks: Global locations and controls. *Remote Sensing Of Environment*, *134*, 294–304. https://doi.org/10.1016/j.rse.2013.03.008

Fenner, D., Bechtel, B., Demuzere, M., Kittner, J., & Meier, F. (2021). CrowdQC+—A Quality-Control for Crowdsourced Air-Temperature Observations Enabling World-Wide Urban Climate Applications. *Frontiers in Environmental Science*, *9*. https://doi.org/10.3389/fenvs.2021.720747

Gemeente Amsterdam. (2020). *Strategie Klimaatadaptatie Amsterdam*. Consulted on 27 June 2025, from https://openresearch.amsterdam/image/2020/3/4/strategie_klimaat_adaptie.pdf

Gemeente Amsterdam. (2021). *Omgevingsvisie 2050 - een menselijke metropool*. Consulted on 27 June 2025, from https://openresearch.amsterdam/nl/page/72317/omgevingsvisie---amsterdam-2050

Heaviside, C., Vardoulakis, S., & Cai, X. (2016a). Attribution of mortality to the urban heat island during heatwaves in the West Midlands, UK. *Environmental Health*, *15*(S1). https://doi.org/10.1186/s12940-016-0100-9

Herbermann, P. (2025). Urban Climate: Mapping Land Surface Temperature Combined with Air Temperature in Amsterdam, Netherlands. *Vrije Universiteit Amsterdam*

Howard, L. (1833). *The Climate of London: Deduced from Meteorological Observations Made in the Metropolis and at Various Places Around it*.

Intergovernmental Panel on Climate Change. (2023). *Climate change 2023: Synthesis report. Contribution of Working Groups I, II and III to the Sixth Assessment Report of the Intergovernmental Panel on Climate Change* (Core Writing Team, H. Lee & J. Romero, Eds.). IPCC. https://doi.org/10.59327/ipcc/ar6-9789291691647

Prata, A. J., Caselles, V., Coll, C., Sobrino, J. A., & Ottlé, C. (1995b). Thermal remote sensing of land surface temperature from satellites: Current status and future prospects. *Remote Sensing Reviews*, *12*(3–4), 175–224. https://doi.org/10.1080/02757259509532285

Khanh, D. N., Varquez, A. C. G., & Kanda, M. (2025). Impact of Anthropogenic Heat on Air Temperature: A First-Order Estimate Using Dimensional Analysis and Numerical Simulations. *Geophysical Research Letters*, *52*(11). https://doi.org/10.1029/2024gl114400

Koninklijk Nederlands Meteorologisch Instituut (KNMI). (2025, 27 February). *KNMI - De Noordzee warmt op*. Consulted on 26 June 2025, from https://www.knmi.nl/over-het-knmi/nieuws/temperature-north-sea-warming-opwarming-noordzee-klimaatveranderingnederland

Koninklijk Nederlands Meteorologisch Instituut (KNMI). (2024, 24 July). *Vijf jaar na het nationale hitterecord van 40,7°C*. Consulted on 6 May 2025, from https://www.knmi.nl/over-het-knmi/nieuws/vijf-jaar-na-het-nationale-hitterecord-van-40-7

Koomen, E., & Diogo, V. (2015). Assessing potential future urban heat island patterns following climate scenarios, socio-economic developments and spatial planning strategies. *Mitigation And Adaptation Strategies For Global Change*, *22*(2), 287–306. https://doi.org/10.1007/s11027-015-9646-z

Krayenhoff, E. S., & Voogt, J. A. (2010). Impacts of Urban Albedo Increase on Local Air Temperature at Daily–Annual Time Scales: Model Results and Synthesis of Previous Work. *Journal Of Applied Meteorology And Climatology*, *49*(8), 1634–1648. https://doi.org/10.1175/2010jamc2356.1

Li, D., & Bou-Zeid, E. (2013). Synergistic Interactions between Urban Heat Islands and Heat Waves: The Impact in Cities Is Larger than the Sum of Its Parts. *Journal Of Applied Meteorology And Climatology*, *52*(9), 2051–2064. https://doi.org/10.1175/jamc-d-13-02.1

Li, L., Zha, Y., & Wang, R. (2020). Relationship of surface urban heat island with air temperature and precipitation in global large cities. *Ecological Indicators*, *117*, 106683. https://doi.org/10.1016/j.ecolind.2020.106683

Liang, S. (2001). Narrowband to broadband conversions of land surface albedo I. *Remote Sensing Of Environment*, *76*(2), 213–238. https://doi.org/10.1016/s0034-4257(00)00205-4

Luber, G., & McGeehin, M. (2008). Climate Change and Extreme Heat Events. *American Journal Of Preventive Medicine*, *35*(5), 429–435. https://doi.org/10.1016/j.amepre.2008.08.021

Marcotullio, P. J., Keßler, C., Gonzalez, R. Q., & Schmeltz, M. (2021). Urban Growth and Heat in Tropical Climates. *Frontiers in Ecology And Evolution*, *9*. https://doi.org/10.3389/fevo.2021.616626

Meier, F., Fenner, D., Grassmann, T., Otto, M., & Scherer, D. (2017). Crowdsourcing air temperature from citizen weather stations for urban climate research. *Urban Climate*, *19*, 170–191. https://doi.org/10.1016/j.uclim.2017.01.006

Mohajerani, A., Bakaric, J., & Jeffrey-Bailey, T. (2017). The urban heat island effect, its causes, and mitigation, with reference to the thermal properties of asphalt concrete. *Journal Of Environmental Management*, *197*, 522–538. https://doi.org/10.1016/j.jenvman.2017.03.095

Naserikia, M., Hart, M. A., Nazarian, N., Bechtel, B., Lipson, M., & Nice, K. A. (2023). Land surface and air temperature dynamics: The role of urban form and seasonality. *The Science Of The Total Environment*, *905*, 167306. https://doi.org/10.1016/j.scitotenv.2023.167306

Oke, T. R. (1982). The energetic basis of the urban heat island. *Quarterly Journal Of The Royal Meteorological Society*, *108*(455), 1–24. https://doi.org/10.1002/qj.49710845502

Paravantis, J., Santamouris, M., Cartalis, C., Efthymiou, C., & Kontoulis, N. (2017). Mortality Associated with High Ambient Temperatures, Heatwaves, and the Urban Heat Island in Athens, Greece. *Sustainability*, *9*(4), 606. https://doi.org/10.3390/su9040606

Perini, K., & Magliocco, A. (2014). Effects of vegetation, urban density, building height, and atmospheric conditions on local temperatures and thermal comfort. *Urban Forestry & Urban Greening*, *13*(3), 495–506. https://doi.org/10.1016/j.ufug.2014.03.003

Phelan, P. E., Kaloush, K., Miner, M., Golden, J., Phelan, B., Silva, H., & Taylor, R. A. (2015). Urban Heat Island: Mechanisms, Implications, and Possible Remedies. *Annual Review Of Environment And Resources*, *40*(1), 285–307. https://doi.org/10.1146/annurev-environ-102014-021155

Prado, R. T. A., & Ferreira, F. L. (2004). Measurement of albedo and analysis of its influence the surface temperature of building roof materials. *Energy And Buildings*, *37*(4), 295–300. https://doi.org/10.1016/j.enbuild.2004.03.009

Schatz, J., & Kucharik, C. J. (2015). Urban climate effects on extreme temperatures in Madison, Wisconsin, USA. *Environmental Research Letters*, *10*(9), 094024. https://doi.org/10.1088/1748-9326/10/9/094024

Scott, A. A., Waugh, D. W., & Zaitchik, B. F. (2018). Reduced Urban Heat Island intensity under warmer conditions. *Environmental Research Letters*, *13*(6), 064003. https://doi.org/10.1088/1748-9326/aabd6c

Shen, L., Guo, X., & Xiao, K. (2014). Spatiotemporally characterizing urbantemperatures based on remote sensing and GISanalysis: a case study in the city of Saskatoon(SK, Canada). *Open Geosciences*, *7*(1). https://doi.org/10.1515/geo-2015-0005

Shiflett, S. A., Liang, L. L., Crum, S. M., Feyisa, G. L., Wang, J., & Jenerette, G. D. (2016). Variation in the urban vegetation, surface temperature, air temperature nexus. *The Science Of The Total Environment*, *579*, 495–505. https://doi.org/10.1016/j.scitotenv.2016.11.069

Sobrino, J. A., Jimenez-Munoz, J. C., Soria, G., Romaguera, M., Guanter, L., Moreno, J., Plaza, A., & Martinez, P. (2008). Land Surface Emissivity Retrieval From Different VNIR and TIR Sensors. *IEEE Transactions On Geoscience And Remote Sensing*, *46*(2), 316–327. https://doi.org/10.1109/tgrs.2007.904834

Stoll, M. J., & Brazel, A. J. (1992). Surface–air temperature relationships in the urban environment of Phoenix, Arizona. *Physical Geography*, *13*(2), 160–179. https://doi.org/10.1080/02723646.1992.10642451

Stone, B., Hess, J. J., & Frumkin, H. (2010). Urban Form and Extreme Heat Events: Are Sprawling Cities More Vulnerable to Climate Change Than Compact Cities? *Environmental Health Perspectives*, *118*(10), 1425–1428. https://doi.org/10.1289/ehp.0901879

United Nations. (2010). *Natural hazards, unnatural disasters: The Economics of Effective Prevention*. World Bank Publications.

Voogt, J., & Oke, T. (2003). Thermal remote sensing of urban climates. *Remote Sensing Of Environment*, *86*(3), 370–384. https://doi.org/10.1016/s0034-4257(03)00079-8

Weng, Q. (2009). Thermal infrared remote sensing for urban climate and environmental studies: Methods, applications, and trends. *ISPRS Journal Of Photogrammetry And Remote Sensing*, *64*(4), 335–344. https://doi.org/10.1016/j.isprsjprs.2009.03.007

White-Newsome, J. L., Brines, S. J., Brown, D. G., Dvonch, J. T., Gronlund, C. J., Zhang, K., Oswald, E. M., & O'Neill, M. S. (2013). Validating Satellite-Derived Land Surface Temperature with in Situ Measurements: A Public Health Perspective. *Environmental Health Perspectives*, *121*(8), 925–931. https://doi.org/10.1289/ehp.1206176

Zanaga, D., Van de Kerchove, R., De Keersmaecker, W., Souverijns, N., Brockmann, C., Quast, R., Wevers, J., Grosu, A., Paccini, A., Vergnaud, S., Cartus, O., Santoro, M., Fritz, S., Georgieva, I., Lesiv, M., Carter, S., Herold, M., Li, L., Tsendbazar, N., . . . Arino, O. (2021). ESA WorldCover 10 m 2020 v100 [Dataset]. In *Zenodo (CERN European Organization for Nuclear Research)*. https://doi.org/10.5281/zenodo.5571936

Zhao, L., Lee, X., Smith, R. B., & Oleson, K. (2014). Strong contributions of local background climate to urban heat islands. *Nature*, *511*(7508), 216–219. https://doi.org/10.1038/nature13462

Zhou, D., Xiao, J., Bonafoni, S., Berger, C., Deilami, K., Zhou, Y., Frolking, S., Yao, R., Qiao, Z., & Sobrino, J. A. (2018). Satellite Remote Sensing of Surface Urban Heat Islands: Progress, Challenges, and Perspectives. *Remote Sensing*, *11*(1), 48. https://doi.org/10.3390/rs11010048